European **J**ournal of **Chem**istry

Quinoline analogue as a potential inhibitor of SARS-CoV-2 main protease: ADMET prediction, molecular docking and dynamics simulation analysis

Praveen Kumar [ID] 1, Santhosha Sangapurada Mahantheshappa [ID] 2,
Sakthivel Balasubramaniyan [ID] 3, Nayak Devappa Satyanarayan [ID] 2 and Rajeshwara Achur [ID] 1,*

1 *Department of Biochemistry, Kuvempu University, Jnana Sahyadri-577451, Shimoga, Karnataka, India*
2 *Department of Pharmaceutical Chemistry, Kuvempu University Post Graduate Centre, Kadur-577458, Chikkamagaluru district, Karnataka-577458, India*
3 *Drug Discovery and Development Research Group, Department of Pharmaceutical Technology, University College of Engineering, Anna University, Tiruchirapalli-62024, Tamilnadu, India*

* *Corresponding author at: Department of Biochemistry, Kuvempu University, Jnana Sahyadri-577451, Shimoga, Karnataka, India.*
 e-mail: rajachur@gmail.com (R. Achur).

RESEARCH ARTICLE

ABSTRACT

The novel coronavirus (COVID-19) has triggered a major human turmoil worldwide by posing challenges regarding infection prevention, disease diagnosis, and treatment. Several drugs including remdesivir (RDV), hydroxychloroquine (HCQ), and others are being used to treat COVID-19, although these are not specifically proven drugs. Thus, it is very critical to understand COVID-19 drug targets and their interactions with candidate drugs. Here, we attempted *in silico* screening of ten quinoline analogs (Q1-Q10) against the five main proteases of SARS-CoV-2 by docking and dynamics analysis. The prediction of the ADMET profile showed that the best docked quinolines are safe and possess drug-like properties. The molecular interaction and binding affinity of these small molecules were determined with respect to the five protease (Mpro) targets of SARS-CoV-2 (PDB ID: 6LU7, 6W63, 6M03, 6Y84 and 6YB7). The study indicated that the quinoline ligands Q4, Q5, Q6, Q7, Q8, Q9, and Q10 as probable inhibitors against SARS-CoV-2 Mpro and showed favorable binding interaction with the amino acid Glu166 of 6Y84, 6LU7 and 6M03. Furthermore, Q9 has a highly significant docking score and binding affinity with all five COVID-19 receptors having a minimum of two H-bonds, which is remarkable compared to HCQ, RDV, and other quinolines. The dynamics simulation analysis of this potent drug candidate Q9 with 6LU7 indicated high stability of the complex. In conclusion, our findings indicate that all of these quinolines in general possess good binding affinity and Q9 can serve as a good quinoline scaffold for the design of new antiviral agents to target the active site of SARS-CoV-2 Mpro.

1. Introduction

The novel coronavirus SARS-CoV-2 is the causative agent responsible for "COVID-19" viral pneumonia outbreak which was first detected in China during 2019-2020 [1]. COVID-19 infection has become a serious public health concern around the world. According to the United States Food and Drug Administration (FDA), there are several COVID-19 treatments currently authorized for emergency use and there are only a few viable treatment options [2]. To test their antiviral effectiveness by repurposing, many drugs are undergoing clinical trials including hydroxychloroquine (HCQ), chloroquine (CQ), and remdesivir (RDV) [3]. Based on the preliminary clinical trial findings and cell culture studies [4], the widely used 70-year-old malaria medications, CQ and HCQ, have been found to exhibit potential therapeutic efficacy against COVID-19 [5]. In addition, RDV, a nucleoside analogue, has also been used against COVID-19 infection [6]. RDV has a wide spectrum of activities in cell cultures and animal models against RNA viruses such as MERS and SARS and was tested in a clinical trial for Ebola [7,8]. RDV has also shown its antiviral potential

against SARS-CoV-2 *in vitro* with an estimated 50% effective concentration at 23.15μM [9]. In mediating viral replication and transcription, CQ plays a key role and makes this virus as an appropriate target [10]. The CQ may also interfere with viral particles that attach to their cellular cell surface receptors by inhibiting a step before the viral cycle [11]. HCQ is a drug that is less toxic and safe to against COVID-19 pneumonia, with increasing reports supporting its use in patients with moderate to severe diseases. The advantage of HCQ is that it can be used in high doses for long periods with very good tolerance levels [12]. *In vitro*, CQ appears as a versatile bioactive agent that has antiviral activity [13] against RNA viruses as diverse as Rabies virus [14], Poliovirus [15], HIV [16], Hepatitis A virus [17], Zika virus [18] and Ebola virus [19]. Regarding corona viruses, the potential therapeutic benefits of CQ were notably reported for SARS-CoV-1 [10,21]. Considering the specific chemical structures and mechanisms of action of CQ and HCQ as weak bases and their immunomodulatory activity, HCQ molecule may be a strong likely candidate for the treatment of COVID-19 infections. However, currently, the study of HCQ is limited to clinical trials and, based on its use outside of clinical trials, risks, and
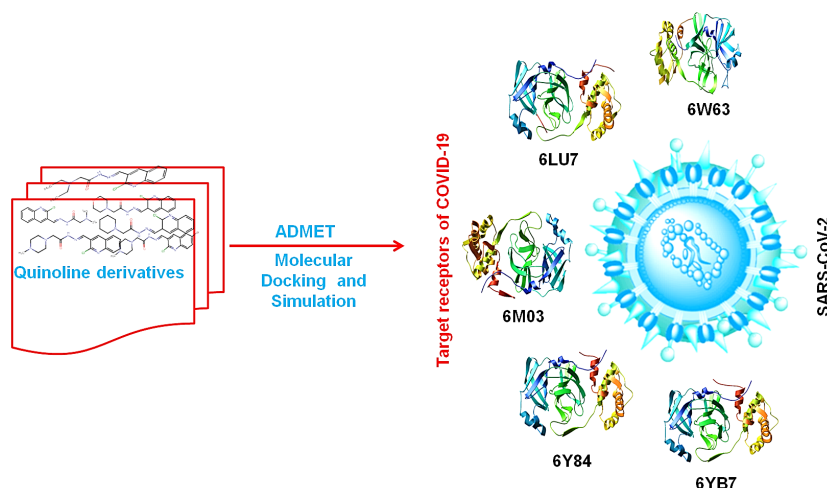
Figure 1. The scheme portrays the detection of active quinoline analogues against five specific Main Proteases of SARS-CoV-2. Mpro structures were obtained from the RCSB protein data bank.
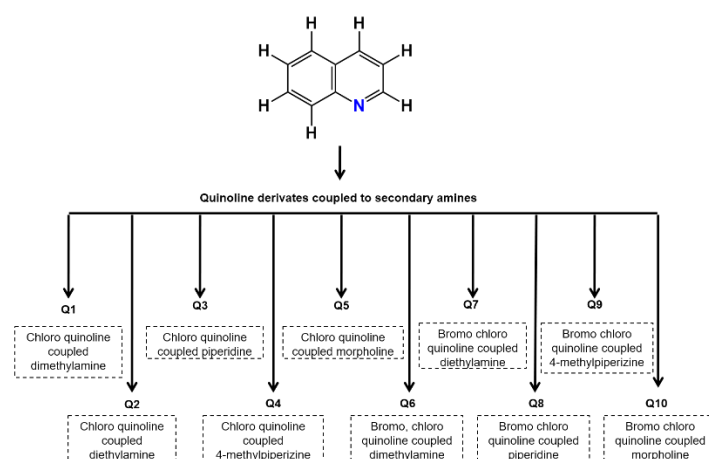

Figure 2. Schematic representation of the broad structural characteristics of ten quinoline derivatives [29].

advantages, there is still a strong beneficial impact to be shown [22]. Therefore, several clinical research registers for the use of HCQ in the treatment of COVID-19 have been listed in the Chinese Clinical Trial Registry (http://www.chictr.org.cn) [23]. In addition, there is still a lack of clinical evidence to show that CQ is as effective as HCQ for the treatment of COVID-19 infection [24,25]. Therefore, the widely used antimalarial CQ and, more importantly, HCQ have been portrayed to deal with COVID-19 threats in travelers who commute between endemic and nonendemic regions [26].

Keeping in view of the lack of proper treatment, it is essential to look for specific potential drugs against COVID-19 infection and the biological efficacy of quinoline ring system being effective against COVID-19 (CQ and HCQ). It has been shown that main protease is a key enzyme of corona viruses, which plays an essential role in several vital cell processes to build it as an attractive drug target for COVID-19 [27]. In this direction, a series of ten quinoline analogues were chosen to study their ADME properties using Schrodinger QikProp software and to compare their drug-likeness properties and medicinal chemistry friendliness with known drug molecules. Recently, we have shown that some of these derivatives are highly effective in inhibiting breast cancer and colorectal cancer cells *in vitro* [28]. In this study, we attempted to determine the efficacy of these quinoline analogues against five specific main proteases of SARS-CoV-2 (Figure 1). The binding affinity interactions of these quinolines were compared with RDV and

HCQ against SARS-CoV-2 proteases to evaluate their efficacy. The structures of the main proteases of the SARS-CoV-2 virus (PDB ID: 6LU7, 6W63, 6M03, 6Y84 and 6YB7) were used to generate receptor grids for docking and to determine the center of the active site for the binding efficacy comparison between the quinolines with that of RDV and HCQ. These studies have shown that, among the ten quinolines, molecule Q9 was found to be the most potent inhibitor of all these main proteases. Furthermore, the stability of Q9 inside the active site of Mpro (PDB 6LU7) was further investigated by molecular dynamics simulation analysis.

2. Experimental

2.1. Quinolines as potential drug molecules

We have used ten quinoline analogs that are available in our small molecules library to carry out the present investigation, which is depicted in Figure 2. These molecules were synthe-sized in our laboratory as previously published [29].

2.2. Ligand preparation and analysis

For *in silico* analysis, the structures of the quinoline molecules were drawn using the Marvin Sketch tool and the SMILES format was extracted for further prediction [30].

Table 1. QIKPROP 3.4 prediction of ADMET values of quinoline analogs.

# of stars	Q1	Q2	Q3	Q4	Q5	Q6	Q7	Q8	Q9	Q10	Recommended value
	0	0	0	0	0	0	0	0	0	0	0-5
CNS	1	1	1	1	1	1	1	1	2	1	−2 (inactive), +2 (active)
MW	290.750	318.805	332.832	346.859	334.805	369.648	397.701	409.712	424.727	411.685	130–725
Dipole	9.881	9.490	9.433	5.564	8.809	8.639	8.333	4.534	8.049	3.801	1.0–12.5
SASA	582.576	627.028	659.946	679.513	628.960	611.660	656.071	674.964	690.538	643.975	300.0–1000.0
Donor HB	1	1	1	1	1	1	1	1	1	1	0.0–6.0
Accept HB	5.5	5.5	5.5	5.5	7.2	5.5	5.5	5.5	7.5	7.2	2.0–20.0
QPlogPoct	15.946	16.495	17.598	17.522	17.837	16.423	17.046	17.385	19.474	17.657	8.0–35.0
QPlogPw	9.053	8.570	9.095	9.062	10.700	8.822	8.338	8.969	10.998	10.574	4.0–45.0
QPlogBB	0.015	0.103	-0.160	-0.069	-0.128	0.184	0.278	0.131	0.516	0.158	-3.0–1.2
IP (eV)	8.917	8.883	8.986	8.843	9.015	9.066	9.030	9.053	9.099	9.097	7.9– 0.5
EA (eV)	1.216	1.187	1.258	1.112	1.288	1.386	1.357	1.344	1.413	1.380	-0.9–1.7
Human oral absorption	3	3	3	3	3	3	3	3	3	3	1, 2, or 3 for low, medium, or high
%Human oral absorption in GI	89.020	100	91.596	95.012	85.581	92.328	100	96.252	78.831	90.305	>80% is high
PSA	65.213	62.687	78.825	78.862	88.295	65.229	62.689	65.994	70.681	75.465	7.0–200.0
Rule of five	0	0	0	0	0	0	0	0	0	0	Maximum is 4
Rule of three	0	0	0	0	0	0	0	0	0	0	Maximum is 3

The chemical structures of HCQ and RDV were extracted from the DRUGBANK database in two-dimensional MDL/MOL format [31]. The SMILES was also submitted to the QikProp tool for ADME prediction. All ligands were subjected to energy minimization and a PDBQT file was generated using the PRODRG (http://prodrg1.dyndns.org/submit.html) web server [32].

2.3. Protein preparation

In general, prior to docking, protein crystal structures are programmed to add hydrogen atoms, optimize the hydrogen bonds, eliminate atomic disagreements, and perform other operations that are not part of the process of configuration of the x-ray crystal structure [33]. The structures of COVID-19 main proteases were obtained from RCSB Protein Data Bank (https://www.pdb.org). We have chosen the crystal structures of all five COVID-19 M^pro that have been recently deposited and available in the Protein Data Bank. Both unliganded and liganded forms of proteins were selected (PDB ID: 6LU7 [34], 6W63 [35], 6M03 [36], 6YB7 [37] and 6Y84 [38]). All water molecules were removed, and polar hydrogen atoms were added to the target protein molecule.

2.4. Prediction of active sites

Ligand binding sites are the active regions of receptors that control protein functionalities. Therefore, the finding of specific binding sites is the first step in studying the functions of proteins and structure-based drug design. MetaPocket program offers a systematic approach to identify ligand-binding sites using eight methods. They are SURFNET, Fpocket, LIGSITE, ConCavity, Move, POC ASA, Q-Site finder and GHECOM. We have used the MetaPocket web server, which has already been widely used to predict binding sites [39-40].

2.5. Molecular docking and analysis

The structure of the target M^pro of COVID-19 (PDB ID: 6LU7, 6W63, 6M03, 6YB7and6Y84) was derived from the Protein Data Bank. These target receptors were performed with Chimera 5.3.1 software (RBVI, Resource for Biocomputing, Visualization and Informatics, University of California, CA, USA, www.cgl.ucsf.edu/chimera/) [41]. Docking studies were performed with AutoDock 4.2 software (https://autodock.scripps.edu/) provided with AutoDock Tools 1.5.4 graphical interface [42]. For the analysis of receptor-ligand interactions, an *in silico* screening pipeline was designed.

2.6. Prediction of ADME descriptors and toxicity of quinoline derivatives.

The main reason why most drug candidates fail during clinical trials is the low ADME and a high toxicity profile. Thus, in the early stages of drug development, an important element of drug research is to determine the essential physio-chemical and toxicity profile of the molecule [43]. QikProp calculates the ADME properties (absorption, distribution, metabolism, and excretion) of quinoline analogues to predict their drugability. The QikProp 3.4 tool was used to predict pharmaceutically and physically significant descriptors with relevant ADME properties and toxicity. These descriptors were calculated for all quinoline molecules and compared with optimal range and found that all derivatives possessed a significant number of hydrogen bond donors and acceptors.

2.7. Molecular dynamic simulation

The molecular dynamic simulation analysis for the best ligand with receptors was carried out using BIOVIA Discovery Studio version 2017. The protocol for standard dynamic cascade and minimization analysis was followed as previously described [44].

3. Results and discussion

3.1. ADME and toxicity studies

To determine the ADMET properties (Absorption, Distribution, Metabolism, Excretion, and Toxicity) of compounds, physicochemical parameters play an important role [45]. In the area of drug development, the evaluation of the basic physiochemical and toxicity profile of the molecule is an important aspect of drug research [43]. This is very critical to their successful biological activity and bioavailability when considering the administration of drugs orally or by any route with real therapeutic potential [46].

In this study, to pick a potential drug candidate, all ten quinoline ligands were screened using QikProp, Schrodinger 2011 software version 3.4 for ADME and toxicity filteration[47]. The QikProp results of ADME were found within the rule of 5 range without violation. The results obtained from this indicate a value of >85% similarity with the known drug molecules (supplementary Table 1). The ADMET predictions of these analogues are asgiven in Table 1. These indicators have shown very good hydrogen bonding ability and oral absorption capacity for all quinolines and thus could be likely drug

Table 2. Molecular interaction between the hit quinoline ligands and the main protease receptors of SARS CoV-2.

No	Compound	Binding energy	Ligand efficiency	Inhibition constant (μM)	No of H	AA in the binding site	H-bond length in Å
PDB-6LU7							
1	Q_9	-5.69	-0.23	67.79	2	LEU 167	2.078
						GLU 166	2.151
2	Q_{10}	-5.73	-0.24	63.35	1	GLU 166	2.015
3	HCQ	-3.84	-0.17	1540	1	PHE 140	2.100
4	RDV	1.90	0.05	-3.17	-	-	-
PDB-6M03							
1	Q_4	-6.96	-0.29	7.95	3	GLU 166	1.760
						GLN 189	2.156
						GLU 166	1.734
2	Q_9	-6.49	-0.26	17.37	2	GLN 189	1.806
						GLU 166	1.885
3	HCQ	-5.65	-0.25	72.30	2	GLY 143	1.890
						GLU 166	2.030
4	RDV	-5.33	-0.13	124.88	1	GLU166	1.945
PDB-6W63							
1	Q_9	-6.97	-0.28	7.76	2	SER 46	1.749
						SER 46	1.959
2	Q_{10}	-5.94	-0.25	44.52	2	THR 24	1.939
						SER 46	1.872
3	HCQ	-4.49	-0.20	514.35	1	THR25	1.847
4	RDV	-5.05	-0.12	198.00	-	-	-
PDB-6Y84							
1	Q_8	-9.87	-0.41	0.058	2	PHE 140	1.900
						GLU 166	1.974
2	Q_9	-8.78	-0.35	0.36	2	GLU 166	1.744
						PHE 140	1.978
3	HCQ	-6.06	-0.26	35.93	2	GLY 143	2.107
						GLU 166	2.029
4	RDV	-7.22	-0.17	5.12	1	GLU166	1.875
PDB-6YB7							
1	Q_8	-6.16	-0.26	30.52	1	HIS 41	2.184
2	Q_9	-6.88	-0.28	9.09	3	THR 24	2.127
						THR 24	2.073
						THR 26	1.837
3	Q_{10}	-6.36	-0.27	21.71	3	THR 24	2.172
						THR 24	1.791
						THR 26	2.096
4	HCQ	-4.88	-0.21	264.33	2	GLY 143	1.838
						ASN 119	
5	RDV	-5.01	-0.12	213.81	3	THR24	1.933
						THR26	1.959
						GLY143	1.725

candidates which are also substantiated by the star value of zero. Furthermore, the number of violations (Lipinski's rule of five and Jorgensen's rule of three) were found to zero for all these molecules. Therefore, most of the predicted pharmacokinetic parameters of these ten quinoline derivatives were found to be within the range or recommended values (Table 1) to become a potent inhibitor drug molecule.

A Polar Surface Area (PSA) of less than 90 angstroms is usually required for drug candidates to penetrate the blood-brain barrier (BBB) and thus act on receptors in the central nervous system. Log BB is the most familiar numeric value that describes permeability through the BBB [48]. Most drugs are not especially permeable through Caco-2 cells [49]. The predicted Caco-2 permeability for these ten quinolines were found to be high for human intestinal absorption (HIA ≥ 80), which authenticates the higher oral absorption or membrane permeability nature of the quinolines. The ADMET prediction result was validated with the docking study results, and these quinolines were found to be nontoxic, absorb in the human intestine, non-carcinogenic, have Caco-2 permeability, and do not violate the Lipinski's rule of three and five, suggesting their significant pharmacokinetic properties.

3.2. Molecular docking studies of quinolines

To understand the binding interaction of these molecules with COVID-19 virus Mpro, molecular docking studies were used. In viral gene expression and replication, Mpros are the main enzymes [50]. Molecular docking studies were performed to investigate the binding efficiency at the active sites of five SARS-CoV-2 Mpro (PDB ID: 6LU7, 6W63, 6M03, 6YB7, and 6Y84). The results of the docking analysis showed that the binding pocket of these COVID-19 proteases involves various amino acid residues such as Ser46 and Thr25 in 6W63; Glu166, Gly189, Asn142, and Gly143 in 6M03; Phe140, Leu167, and Glu166 in 6LU7; Glu166, Phe140, and Gly143 in 6Y84[51] and Cys44, Thr24, Thr26, His41, Gly143, and Asn119 in 6YB7. The important hydrogen bond forming amino acid residues are Glu166, Phe140 and Asn142. It has already been shown that His41, His163, His164, and Glu166 are the most important amino acid residues of COVID-19 Mpro in the interaction with the inhibitor in the case of the 6LU7 receptor using FMO analysis [52]. In this study, the tested quinoline ligands were also found to commonly bind to Glu166 to form a hydrogen bond within a 2.3 Å distance with the receptors 6LU7, 6Y84 and 6M03 (Table 2).

Recently, it has been reported that quinoline 1, 2, 3, 4-tetrahydro-1-[(2-phenylcyclopropyl) sulfonyl]-trans-(8CI) can target main proteases through interaction with His41 of SARS-CoV-2 Mpro 6LU7 [53]. Similarly, our docking study of molecule Q8 against 6YB7 was found to have binding interaction with His41 and forms the 2.1Å hydrogen bond. On the other hand, standard drug molecules, HCQ and RDV, bind to the active site amino acids of the five Mpro implicated in COVID-19. However, the binding to residues His41 and Glu166 of Mpro could be an important factor in the inhibition of its protease activity.
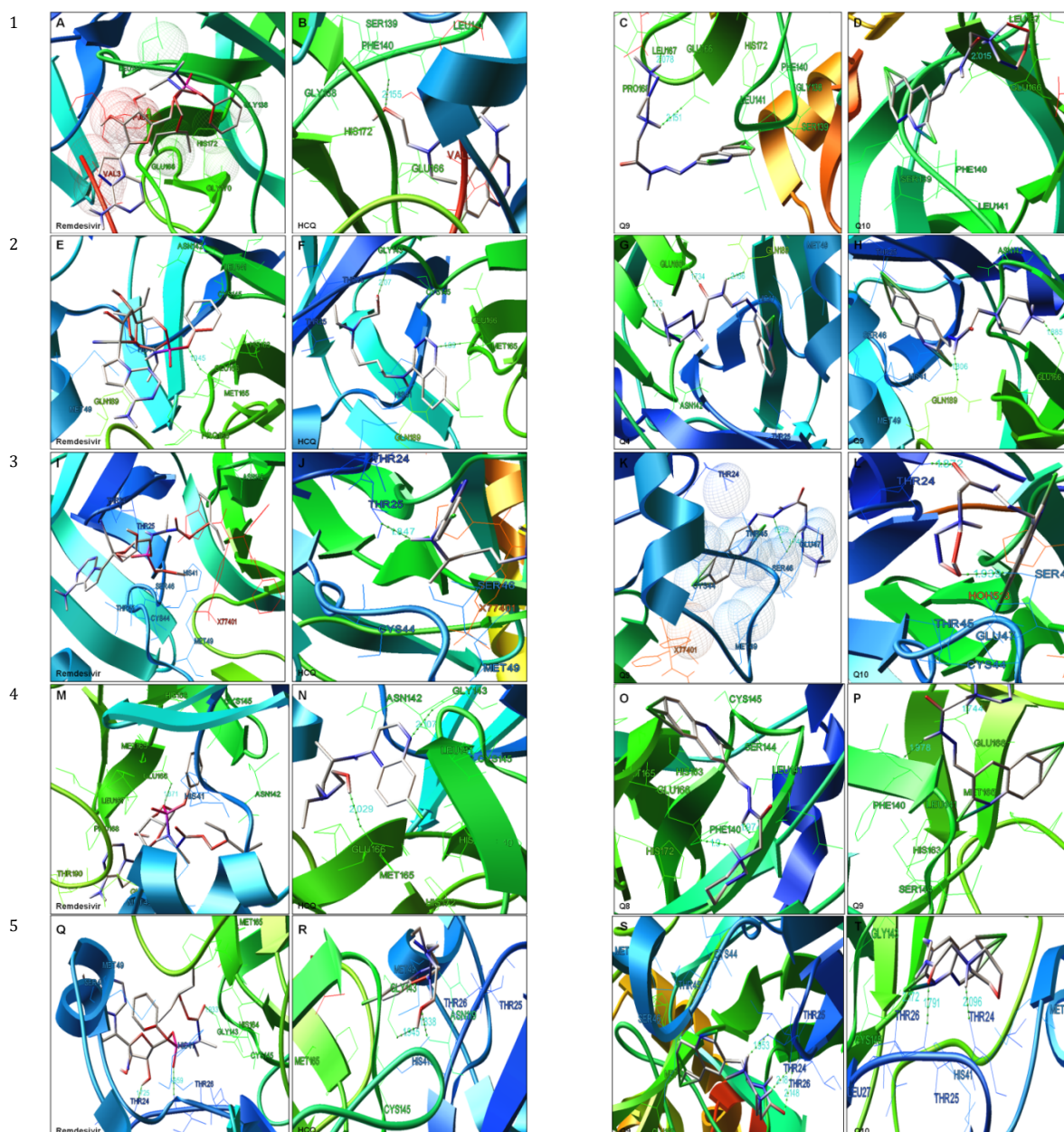
Figure 3. Binding interaction of the hit quinoline derivatives with COVID-19 Mᵖʳᵒ (PDB ID: 6LU7, 6M03, 6W63, 6Y84 and 6YB7) is shown in rows 1, 2, 3, 4 and 5, respectively. The green dotted line indicates the hydrogen bond. The panels A, E, I, M and Q represent interaction with RDV, panels B, F, I, N and R represent interaction with HCQ, panels C, G, K, O and S represent interaction with Q9, Q4, Q9, Q8 and Q9, and panels D, H, L, P and T indicate the interaction with Q10, Q9, Q10, Q9 and Q10, respectively.

We also analyzed the protein-ligand complexes to better understand the interactions between protein residues and the bound ligands, along with the binding site residues of the defined receptor. Binding of the quinoline analogues, HCQ and RDV, with Mᵖʳᵒ of the COVID-19 receptors indicated the spontaneity of binding as confirmed by the negative values of free energies and H-bond formation. Among several ligand molecules, the highly potent ligands with the highest binding energy with each of the Mᵖʳᵒ are shown in Table 2.

The data obtained here indicate that the compound Q9 interacts more effectively with the five Mᵖʳᵒ of COVID-19 and forms two or more hydrogen bonds with each target receptor; the binding energy ranged from -8.78 to-5.94 kcal/mol. The binding interactions between other quinoline derivatives with the target receptors 6LU7, 6Y84, and 6M03 were also found to be in the negative range, indicating a significant interaction involving the binding with the most important amino acid residue Glu166 of Mᵖʳᵒ. Furthermore, the standard drug molecule HCQ was also found to interact with Glu166 of 6M03 and 6Y84 receptors. The binding energy of HCQ to the five receptors ranged from -6.06 to -3.84kcal/mol (Table 2). Based on the binding energy and H-bond formation, the most potent compounds were found to be Q8 (-9.87 to-3.91 kcal/mol), Q9 (-8.78 to-5.94 kcal/mol) and Q10 (-8.76 to -5.73 kcal/mol). On the other hand, both RDV and HCQ also exhibited the binding interaction with Glu166, but formed less number of H-bonds and weak binding energies as compared to the quinoline analogues (Figure 3).
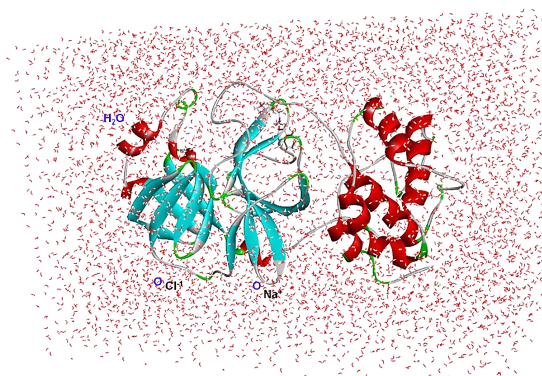
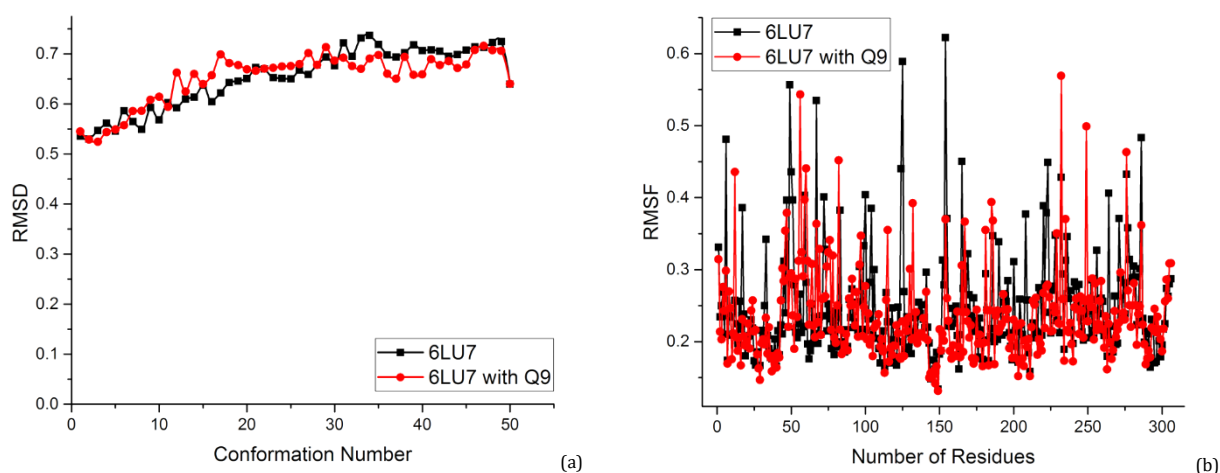**Figure 4.** Solvation process of the 6LU7 and Q9 complexes.

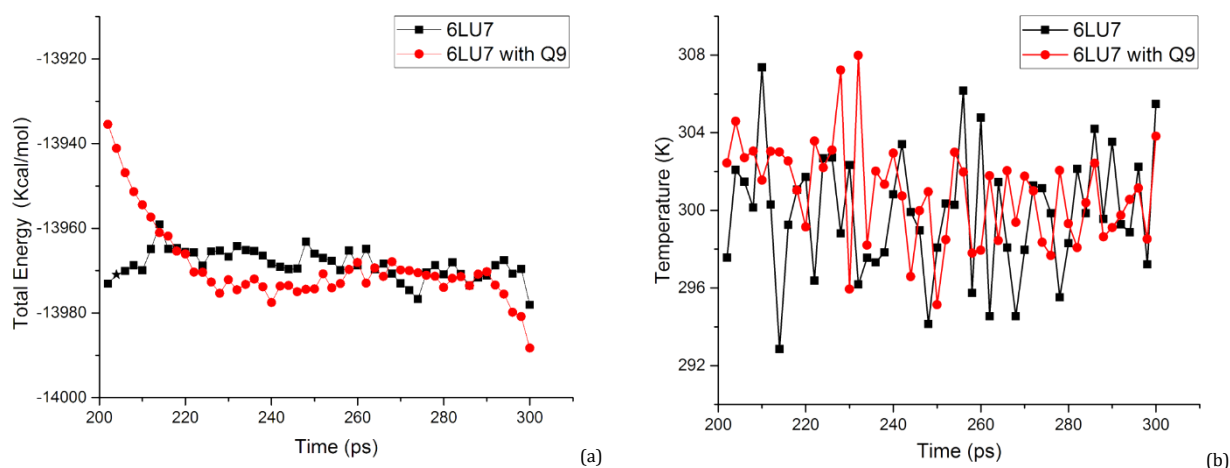**Figure 5.** (a) RMSD and (b) RMSF of various conformations of 6LU7 and its complex residues.

Figure 6. (a) Time based total energy and (b) temperature changes on different time scales of 6LU7 and its complex.

3.3. Molecular dynamic simulation studies

The molecular dynamics (MD) simulation was focused on the lead molecule Q9 as well as Q9 with M^{Pro} of COVID-19 receptor 6LU7. We evaluated the properties of the receptor, the stability of the ligand-receptor complex (6LU7 with Q9), and the conformation changes in different temperatures (K) and energy functions (kcal/mol) The results of molecular docking study suggested that ligand Q9 possesses good binding affinity with the 6LU7 receptor of COVID-19. Thus, we selected this complex protein for further MD analysis to determine the stability

changes. In the solvation process of the explicit periodic border cell, 1247 water molecules, 67 sodium ions and 55 chloride ions were observed. The molecular conformation, electronic properties, and binding energies of the 6LU7 complex were further determined (Figure 4). During the MD simulations, the stability of each conformation of 6LU7 and 6LU7 with Q9 were monitored through the root mean square deviation (RMSD) and root mean square fluctuation (RMSF). The analysis indicates the RMSD values of 1.0 and 0.9 Å for 6LU7 and 6LU7 with Q9, respectively (Figure 5). From the results of the RMSD and RMSF analysis, it is clear that the Q9 ligand does not change the

conformation of 6LU7, including the structure of residues. We have also determined the total energy variation and the stabilization temperature of the protein complex (Figure 6). The receptor was found to stabilize at 210ps time between 300-304K temperatures. Finally, the ligand Q9 does not influence the RMSD and stability of the 6LU7 protein at various temperatures and energy values based on these MD findings.

4. Conclusions

Currently, there are no approved drugs/vaccines for the treatment of COVID-19 infections. In addition to discovering a potent and specific drug, it is urgently needed to develop universal broad-spectrum vaccines against COVID-19 and other SARS or influenza viruses to combat future pandemics. In this direction, we intended to expose the therapeutic potential of certain quinoline derivatives with respect to SARS CoV-2's five main proteases. The molecule bearing quinoline scaffolds is widespread in various potent bioactive natural and synthetic compounds. Quinoline-based antimalarial drugs, such as HCQ and CQ, have shown significant efficacy in the treatment of COVID-19 infections [54,55]. Several quinoline-based drug candidates have been identified to have a connection with COVID-19 or a role in suppressing viral progression and possess a wide range of antiviral activity [56]. The strong safety profile of aminoquinolines at the currently recommended doses for the prevention or early treatment of COVID-19 is confirmed by evidence from randomized controlled trials (RCTs) [57]. In general, the findings of our study will be helpful in a short list of compounds to be repurposed as a therapeutic candidate against M^{pro} and its mutants.

Essential functional biological macromolecules in coronaviruses are viral proteases. For the effective treatment of several viral diseases, these proteases have been considered as potential drug targets [58]. Therefore, protease inhibitors comprise the majority of reported anti-SARS-CoV-2 drugs. This has influenced us to identify the potential protease inhibitors centered on the quinoline moiety against the SARS-CoV-2 therapeutic targets using an *in silico* approach.

From our library of quinoline compounds, a series of ten compounds were subjected to *in silico* analysis along with standard drug molecules, HCQ and RDV, against the five main proteases of COVID-19. Among the five different main proteases utilized to determine the active amino acid residue, Glu166 has been found to be the most important amino acid of M^{pro} which interacts with the inhibitor [59]. The center of the active site of the grid was determined and the results of these quinolines showed a better binding energy and hydrogen bond formation, indicating that the quinoline analogues Q4, Q6, Q8, Q9 and Q10 have a significantly higher binding interaction with all receptors compared to HCQ and RDV. Among these quinoline molecules, Q9 was found to be a highly potent lead molecule with significant binding interactions with all target receptors of SARS-CoV-2. These interaction parameters are in good agreement with the current evidence to indicate a good pharmacokinetics profile. Furthermore, the MD studies performed in this study for the highly potent drug candidate Q9 also proved that the binding conformational stability with SARS-CoV-2 M^{pro} (PDB ID 6LU7) does not change its nature. The results of our ADMET analysis are also useful in providing insights into the structural criteria for synthesizing a new potential drug molecule with a better inhibitory activity against COVID-19 [60, 61]. Overall, the present work should lead to the identification of novel, less toxic, and highly efficient quinoline derivatives for chemical interventions to manage COVID-19 infections. The use of bioinformatic tools should be helpful in designing and synthesizing more appropriate molecules which can interact better with specific receptors by the combinatorial approach.

Disclosure statement DS

CRediT authorship contribution statement CR

Conceptualization: Praveen Kumar, Rajeshwara Achur; Methodology: Praveen Kumar, Rajeshwara Achur; Software: Praveen Kumar, Sakthivel Balasubramaniyan; Validation: Praveen Kumar, Rajeshwara Achur, Nayak Devappa Satyanarayan; Formal Analysis: Rajeshwara Achur, Nayak Devappa Satyanarayan, Praveen Kumar; Investigation: Praveen Kumar, Rajeshwara Achur; Resources: Nayak Devappa Satyanarayan, Rajeshwara Achur, Santhosha Sangapurada Mahantheshappa; Data Curation: Praveen Kumar, Rajeshwara Achur; Writing - Original Draft: Praveen Kumar; Writing - Review and Editing: Rajeshwara Achur, Nayak Devappa Satyanarayan; Visualization: Praveen Kumar, Sakthivel Balasubramaniyan; Funding acquisition: We have not received any funds to carry out this research work; Supervision: Rajeshwara Achur, Nayak Devappa Satyanarayan.

ORCID iD and Email ✉

Praveen Kumar
✉ praveenbiochemku@gmail.com
iD https://orcid.org/0000-0002-8034-6348
Santhosha Sangapurada Mahantheshappa
✉ santhosh.1507@rediffmail.com
iD https://orcid.org/0000-0001-8734-2991
Sakthivel Balasubramaniyan
✉ sakthivelbala.s@gmail.com
iD https://orcid.org/0000-0003-1066-9878
Nayak Devappa Satyanarayan
✉ satya1782005@gmail.com
iD https://orcid.org/0000-0003-4511-3749
Rajeshwara Achur
✉ rajachur@gmail.com
✉ anr@kuvempu.ac.in
iD https://orcid.org/0000-0001-9867-8917

References

[1]. Yang, P.; Ding, Y.; Xu, Z.; Pu, R.; Li, P.; Yan, J.; Liu, J.; Meng, F.; Huang, L.; Shi, L.; Jiang, T.; Qin, E.; Zhao, M.; Zhang, D.; Zhao, P.; Yu, L.; Wang, Z.; Hong, Z.; Xiao, Z.; Xi, Q.; Zhao, D.; Yu, P.; Zhu, C.; Chen, Z.; Zhang, S.; Ji, J.; Cao, G.; Wang, F. Epidemiological and Clinical Features of COVID-19 Patients with and without Pneumonia in Beijing, China. *BioRxiv*, 2020. https://doi.org/10.1101/2020.02.28.20028068.

[2]. Weiner, D. L.; Balasubramaniam, V.; Shah, S. I.; Javier, J. R.; Pediatric Policy Council. COVID-19 Impact on Research, Lessons Learned from COVID-19 Research, Implications for Pediatric Research. *Pediatr. Res.* **2020**, *88* (2), 148–150.

[3]. Smyth, T.; Ramachandran, V. N.; Smyth, W. F. A Study of the Antimicrobial Activity of Selected Naturally Occurring and Synthetic Coumarins. *Int. J. Antimicrob. Agents* **2009**, *33* (5), 421–426.

[4]. Yazdany, J.; Kim, A. H. J. Use of Hydroxychloroquine and Chloroquine during the COVID-19 Pandemic: What Every Clinician Should Know. *Ann. Intern. Med.* **2020**, *172* (11), 754–755.

[5]. Wang, M.; Cao, R.; Zhang, L.; Yang, X.; Liu, J.; Xu, M.; Shi, Z.; Hu, Z.; Zhong, W.; Xiao, G. Remdesivir and Chloroquine Effectively Inhibit the Recently Emerged Novel Coronavirus (2019-NCoV) in Vitro. *Cell Res.* **2020**, *30* (3), 269–271.

[6]. Gao, J.; Tian, Z.; Yang, X. Breakthrough: Chloroquine Phosphate Has Shown Apparent Efficacy in Treatment of COVID-19 Associated Pneumonia in Clinical Studies. *Biosci. Trends* **2020**, *14* (1), 72–73.

[7]. Li, G.; De Clercq, E. Therapeutic Options for the 2019 Novel Coronavirus (2019-NCoV). *Nat. Rev. Drug Discov.* **2020**, *19* (3), 149–150.

[8]. Vijayalakshmi, P.; Daisy, P. Effective Interaction Studies for Inhibition of DNA Ligase Protein from Staphylococcus Aureus. *J. Recept. Signal Transduct. Res.* **2015**, *35* (1), 15–25.

[9]. Choy, K.-T.; Wong, A. Y.-L.; Kaewpreedee, P.; Sia, S. F.; Chen, D.; Hui, K. P. Y.; Chu, D. K. W.; Chan, M. C. W.; Cheung, P. P.-H.; Huang, X.; Peiris, M.; Yen, H.-L. Remdesivir, Lopinavir, Emetine, and Homoharringtonine Inhibit SARS-CoV-2 Replication in Vitro. *Antiviral Res.* **2020**, *178* (104786), 104786.

[10]. Zhu, N.; Zhang, D.; Wang, W.; Li, X.; Yang, B.; Song, J.; Zhao, X.; Huang, B.; Shi, W.; Lu, R.; Niu, P.; Zhan, F.; Ma, X.; Wang, D.; Xu, W.; Wu, G.; Gao, G. F.; Tan, W.; China Novel Coronavirus Investigating and Research Team. A Novel Coronavirus from Patients with Pneumonia in China, 2019. *N. Engl. J. Med.* **2020**, *382* (8), 727–733.

[11]. Kwiek, J. J.; Haystead, T. A. J.; Rudolph, J. Kinetic Mechanism of Quinone Oxidoreductase 2 and Its Inhibition by the Antimalarial Quinolines. *Biochemistry* **2004**, *43* (15), 4538–4547.

[12]. Devaux, C. A.; Rolain, J.-M.; Colson, P.; Raoult, D. New Insights on the Antiviral Effects of Chloroquine against Coronavirus: What to Expect for COVID-19? *Int. J. Antimicrob. Agents* **2020**, *55* (5), 105938.

[13]. Tsiang, H.; Superti, F. Ammonium Chloride and Chloroquine Inhibit Rabies Virus Infection in Neuroblastoma Cells. *Arch. Virol.* **1984**, *81* (3–4), 377–382.

[14]. Kronenberger, P.; Vrijsen, R.; Boeyé, A. Chloroquine Induces Empty Capsid Formation during Poliovirus Eclipse. *J. Virol.* **1991**, *65* (12), 7008–7011.

[15]. Savarino, A.; Gennero, L.; Sperber, K.; Boelaert, J. R. The Anti-HIV-1 Activity of Chloroquine. *J. Clin. Virol.* **2001**, *20* (3), 131–135.

[16]. Bishop, N. E. Examination of Potential Inhibitors of Hepatitis A Virus Uncoating. *Intervirology* **1998**, *41* (6), 261–271.

[17]. Delvecchio, R.; Higa, L. M.; Pezzuto, P.; Valadão, A. L.; Garcez, P. P.; Monteiro, F. L.; Loiola, E. C.; Dias, A. A.; Silva, F. J. M.; Aliota, M. T.; Caine, E. A.; Osorio, J. E.; Bellio, M.; O'Connor, D. H.; Rehen, S.; de Aguiar, R. S.; Savarino, A.; Campanati, L.; Tanuri, A. Chloroquine, an Endocytosis Blocking Agent, Inhibits Zika Virus Infection in Different Cell Models. *Viruses* **2016**, *8* (12), 322. https://doi.org/10.3390/v8120322.

[18]. Dowall, S. D.; Bosworth, A.; Watson, R.; Bewley, K.; Taylor, I.; Rayner, E.; Hunter, L.; Pearson, G.; Easterbrook, L.; Pitman, J.; Hewson, R.; Carroll, M. W. Chloroquine Inhibited Ebola Virus Replication in Vitro but Failed to Protect against Infection and Disease in the in Vivo Guinea Pig Model. *J. Gen. Virol.* **2015**, *96* (12), 3484–3492.

[19]. Savarino, A.; Boelaert, J. R.; Cassone, A.; Majori, G.; Cauda, R. Effects of Chloroquine on Viral Infections: An Old Drug against Today's Diseases? *Lancet Infect. Dis.* **2003**, *3* (11), 722–727.

[20]. Keyaerts, E.; Li, S.; Vijgen, L.; Rysman, E.; Verbeeck, J.; Van Ranst, M.; Maes, P. Antiviral Activity of Chloroquine against Human Coronavirus OC43 Infection in Newborn Mice. *Antimicrob. Agents Chemother.* **2009**, *53* (8), 3416–3421.

[21]. Cortegiani, A.; Ingoglia, G.; Ippolito, M.; Giarratano, A.; Einav, S. A Systematic Review on the Efficacy and Safety of Chloroquine for the Treatment of COVID-19. *J. Crit. Care* **2020**, *57*, 279–283.

[22]. Fadelelmoula, T. Efficacy and Safety of Hydroxychloroquine in Treating COVID-19 Pneumonia: Uncertainty of Data and Changing Treatment Protocols. *J. Lung Pulm. Respir. Res.* **2020**, *7* (2), 62–65.

[23]. Wu, T.; Li, Y.; Liu, G.; Li, J.; Wang, L.; Du, L.; Chinese Clinical Registry. Chinese Clinical Trial Registry: Mission, Responsibility and Operation: Chinese Clinical Trial Registry: Mission, Responsibility and Operation. *J. Evid. Based Med.* **2011**, *4* (3), 165–167.

[24]. Liu, J.; Cao, R.; Xu, M.; Wang, X.; Zhang, H.; Hu, H.; Li, Y.; Hu, Z.; Zhong, W.; Wang, M. Hydroxychloroquine, a Less Toxic Derivative of Chloroquine, Is Effective in Inhibiting SARS-CoV-2 Infection in Vitro. *Cell Discov.* **2020**, *6* (1), 16.

[25]. Khuroo, M. S. Chloroquine and hydroxychloroquine in coronavirus disease 2019 (COVID-19). Facts, fiction and the hype: a critical appraisal. Int. *J. Antimicrob. Agents* **2020**, *56*, 106101.

[26]. Rodriguez-Valero, N.; Vera, I.; Torralvo, M. R.; De Alba, T.; Ferrer, E.; Camprubi, D.; AlmuedoRiera, A.; Gallego, R. S.; Muelas, M.; Pinazo, M. J.; Muñoz, J. Malaria Prophylaxis Approach during COVID-19 Pandemic. *Travel Med. Infect. Dis.* **2020**, *38* (101716), 101716.

[27]. Wu, C.; Liu, Y.; Yang, Y.; Zhang, P.; Zhong, W.; Wang, Y.; Wang, Q.; Xu, Y.; Li, M.; Li, X.; Zheng, M.; Chen, L.; Li, H. Analysis of therapeutic targets for SARS-CoV-2 and discovery of potential drugs by computational methods. *Acta Pharm. Sin. B.* **2020**, *10*, 766–788.

[28]. Kumar, P.; Uthaiah, C. A.; Mahantheshappa, S. S.; Satyanarayan, N. D.; Madhunapantula, S. V.; Kumar, H. S. S.; Achur, R. Antiproliferative Potential, Quantitative Structure-Activity Relationship, Cheminformatic and Molecular Docking Analysis of Quinoline and Benzofuran Derivatives. *Eur. J. Chem.* **2020**, *11* (3), 223–234.

[29]. Mahantheshappa, S. S.; Shivanna, H.; Satyanarayan, N. D. Synthesis, Antimicrobial, Antioxidant, and ADMET Studies of Quinoline Derivatives. *Eur. J. Chem.* **2021**, *12* (1), 37–44.

[30]. ChemAxon - Software Solutions and Services for Chemistry & Biology, Marvin Sketch.17.21.0 https://www.chemaxon.com (accessed Jul 15, 2021).

[31]. Wishart, D. S.; Feunang, Y. D.; Guo, A. C.; Lo, E. J.; Marcu, A.; Grant, J. R.; Sajed, T.; Johnson, D.; Li, C.; Sayeeda, Z.; Assempour, N.; Iynkkaran, I.; Liu, Y.; Maciejewski, A.; Gale, N.; Wilson, A.; Chin, L.; Cummings, R.; Le, D.; Pon, A.; Knox, C.; Wilson, M. DrugBank 5.0: A Major Update to the DrugBank Database for 2018. *Nucleic Acids Res.* **2018**, *46* (D1), D1074–D1082.

[32]. Schüttelkopf, A. W.; van Aalten, D. M. F. PRODRG: A Tool for High-Throughput Crystallography of Protein-Ligand Complexes. *Acta Crystallogr. D Biol. Crystallogr.* **2004**, *60* (Pt 8), 1355–1363.

[33]. Sastry, G. M.; Adzhigirey, M.; Day, T.; Annabhimoju, R.; Sherman, W. Protein and Ligand Preparation: Parameters, Protocols, and Influence on Virtual Screening Enrichments. *J. Comput. Aided Mol. Des.* **2013**, *27* (3), 221–234.

[34]. Jin, Z.; Du, X.; Xu, Y.; Deng, Y.; Liu, M.; Zhao, Y.; Zhang, B.; Li, X.; Zhang, L.; Peng, C.; Duan, Y.; Yu, J.; Wang, L.; Yang, K.; Liu, F.; Jiang, R.; Yang, X.; You, T.; Liu, X.; Yang, X.; Bai, F.; Liu, H.; Liu, X.; Guddat, L. W.; Xu, W.; Xiao, G.; Qin, C.; Shi, Z.; Jiang, H.; Rao, Z.; Yang, H. Structure of Mpro from SARS-CoV-2 and Discovery of Its Inhibitors. *Nature* **2020**, *582* (7811), 289–293.

[35]. Estrada, E. Topological Analysis of SARS CoV-2 Main Protease. *Chaos* **2020**, *30* (6), 061102.

[36]. Zhang, B.; Zhao, Y.; Jin, Z.; Liu, X.; Yang, H.; Rao, Z. The Crystal Structure of COVID-19 Main Protease in Apo Form. Worldwide Protein Data Bank March 11, 2020. https://doi.org/10.2210/pdb6m03/pdb.

[37]. Douangamath, A.; Fearon, D.; Gehrtz, P.; Krojer, T.; Lukacik, P.; Owen, C. D.; Resnick, E.; Strain-Damerell, C.; Aimon, A.; Ábrányi-Balogh, P.; Brandão-Neto, J.; Carbery, A.; Davison, G.; Dias, A.; Downes, T. D.; Dunnett, L.; Fairhead, M.; Firth, J. D.; Jones, S. P.; Keeley, A.; Keserü, G. M.; Klein, H. F.; Martin, M. P.; Noble, M. E. M.; O'Brien, P.; Powell, A.; Reddi, R. N.; Skyner, R.; Snee, M.; Waring, M. J.; Wild, C.; London, N.; von Delft, F.; Walsh, M. A. Crystallographic and Electrophilic Fragment Screening of the SARS-CoV-2 Main Protease. *Nat. Commun.* **2020**, *11* (1), 5047.

[38]. Owen, C. D.; Lukacik, P.; Strain-Damerell, C. M.; Douangamath, A.; Powell, A. J.; Fearon, D.; Brandao-Neto, J.; Crawshaw, A. D.; Aragao, D.; Williams, M.; Flaig, R.; Hall, D. R.; McAuley, K. E.; Mazzorana, M.; Stuart, D. I.; von Delft, F.; Walsh, M. A. SARS-CoV-2 Main Protease with Unliganded Active Site (2019-NCoV, Coronavirus Disease 2019, COVID-19). Worldwide Protein Data Bank March 11, 2020. https://doi.org/10.2210/pdb6y84/pdb.

[39]. Pandey, A. K.; Siddiqui, M. H.; Dutta, R. Drug-Likeness Prediction of Designed Analogues of Isoniazid Standard Targeting FabI Enzyme Regulation from P. Falciparum. *Bioinformation* **2019**, *15* (5), 364–368.

[40]. Thakur, Z.; Dharra, R.; Saini, V.; Kumar, A.; Mehta, P. K. Insights from the Protein-Protein Interaction Network Analysis of Mycobacterium Tuberculosis Toxin-Antitoxin Systems. *Bioinformation* **2017**, *13* (11), 380–387.

[41]. Goddard, T. D.; Huang, C. C.; Ferrin, T. E. Visualizing Density Maps with UCSF Chimera. *J. Struct. Biol.* **2007**, *157* (1), 281–287.

[42]. Norgan, A. P.; Coffman, P. K.; Kocher, J.-P. A.; Katzmann, D. J.; Sosa, C. P. Multilevel Parallelization of AutoDock 4.2. *J. Cheminform.* **2011**, *3* (1), 12.

[43]. Ray, S.; Madrid, P. B.; Catz, P.; LeValley, S. E.; Furniss, M. J.; Rausch, L. L.; Guy, R. K.; DeRisi, J. L.; Iyer, L. V.; Green, C. E.; Mirsalis, J. C. Development of a New Generation of 4-Aminoquinoline Antimalarial Compounds Using Predictive Pharmacokinetic and Toxicology Models. *J. Med. Chem.* **2010**, *53* (9), 3685–3695.

[44]. Balasubramaniyan, S.; Irfan, N.; Umamaheswari, A.; Puratchikody, A. Design and Virtual Screening of Novel Fluoroquinolone Analogs as Effective Mutant DNA GyrA Inhibitors against Urinary Tract Infection-Causing Fluoroquinolone Resistant Escherichia Coli. *RSC Adv.* **2018**, *8* (42), 23629–23647.

[45]. Kumar, P.; Satyanarayan, N. D.; Madhunapantula, S. R. V.; Kumar, H. S. S.; Achur, R. In Silico Screening for the Interaction of Small Molecules with Their Targets and Evaluation of Therapeutic Efficacy by Free Online Tools. *Eur. J. Chem.* **2020**, *11* (2), 168–178.

[46]. Han, Y.; Zhang, J.; Hu, C. Q.; Zhang, X.; Ma, B.; Zhang, P. In Silico ADME and Toxicity Prediction of Ceftazidime and Its Impurities. *Front. Pharmacol.* **2019**, *10*, 434.

[47]. Small-Molecule Drug Discovery Suite 2013 QikProp, Version 3.8, Schrödinger, LLC, New York, NY, 2013.

[48]. Clark, D. E. Rapid Calculation of Polar Molecular Surface Area and Its Application to the Prediction of Transport Phenomena. 1. Prediction of Intestinal Absorption. *J. Pharm. Sci.* **1999**, *88* (8), 807–814.

[49]. O'Hagan, S.; Kell, D. B. The Apparent Permeabilities of Caco-2 Cells to Marketed Drugs: Magnitude, and Independence from Both Biophysical Properties and Endogenite Similarities. *PeerJ* **2015**, *3* (e1405), e1405.

[50]. Yang, H.; Xie, W.; Xue, X.; Yang, K.; Ma, J.; Liang, W.; Zhao, Q.; Zhou, Z.; Pei, D.; Ziebuhr, J.; Hilgenfeld, R.; Yuen, K. Y.; Wong, L.; Gao, G.; Chen, S.; Chen, Z.; Ma, D.; Bartlam, M.; Rao, Z. Design of Wide-Spectrum Inhibitors Targeting Coronavirus Main Proteases. *PLoS Biol.* **2005**, *3* (10), e324.

[51]. Thakkar, S. S.; Shelat, F.; Thakor, P. Magical bullets from an indigenous Indian medicinal plant Tinosporacordifolia: An in silico approach for the antidote of SARS-CoV-2. *Egyptian J. Petroleum* **2021**, *30*(1), 53–66.

[52]. Hatada, R.; Okuwaki, K.; Mochizuki, Y.; Handa, Y.; Fukuzawa, K.; Komeiji, Y.; Okiyama, Y.; Tanaka, S. Fragment Molecular Orbital Based Interaction Analyses on COVID-19 Main Protease - Inhibitor N3 Complex (PDB ID: 6LU7). *J. Chem. Inf. Model.* **2020**, *60* (7), 3593–3602.

[53]. Alexpandi, R.; De Mesquita, J. F.; Pandian, S. K.; Ravi, A. V. Quinolines-Based SARS-CoV-2 3CLpro and RdRp Inhibitors and Spike-RBD-ACE2 Inhibitor for Drug-Repurposing against COVID-19: An in Silico Analysis. *Front. Microbiol.* **2020**, *11*, 1796.

[54]. Zumla, A.; Chan, J. F. W.; Azhar, E. I.; Hui, D. S. C.; Yuen, K.-Y. Coronaviruses - Drug Discovery and Therapeutic Options. *Nat. Rev. Drug Discov.* **2016**, *15* (5), 327–347.

[55]. Zhang, W.; Zhao, Y.; Zhang, F.; Wang, Q.; Li, T.; Liu, Z.; Wang, J.; Qin, Y.; Zhang, X.; Yan, X.; Zeng, X.; Zhang, S. The Use of Anti-Inflammatory Drugs in the Treatment of People with Severe Coronavirus Disease 2019 (COVID-19): The Perspectives of Clinical Immunologists from China. *Clin. Immunol.* **2020**, *214* (108393), 108393.

[56]. Fantini, J.; Chahinian, H.; Yahi, N. Synergistic Antiviral Effect of Hydroxychloroquine and Azithromycin in Combination against SARS-CoV-2: What Molecular Dynamics Studies of Virus-Host Interactions Reveal. *Int. J. Antimicrob. Agents* **2020**, *56* (2), 106020.

[57]. Schilling, W. H.; White, N. J. Does Hydroxychloroquine Still Have Any Role in the COVID-19 Pandemic? *Expert Opin. Pharmacother.* **2021**, *22* (10), 1257–1266.

[58]. Elfiky, A. A. Ribavirin, Remdesivir, Sofosbuvir, Galidesivir, and Tenofovir against SARS-CoV-2 RNA Dependent RNA Polymerase (RdRp): A Molecular Docking Study. *Life Sci.* **2020**, *253* (117592), 117592.

[59]. Majumder, R.; Mandal, M. Screening of plant-based natural compounds as a potential COVID-19 main protease inhibitor: An *in silico* docking and molecular dynamics simulation approach. *J. Biomol. Struct. Dyn.* **2022**, *40*, 696–711.

[60]. Kajal, K.; Panda, A. K.; Bhat, J.; Chakraborty, D.; Bose, S.; Bhattacharjee, P.; Sarkar, T.; Chatterjee, S.; Kar, S. K.; Sa, G. Andrographolide Binds to ATP-Binding Pocket of VEGFR2 to Impede VEGFA-Mediated Tumor-Angiogenesis. *Sci. Rep.* **2019**, *9* (1), 4073.

[61]. Al-Jaidi, B. A.; Telfah, S. T.; Bardaweel, S. K.; Deb, P. K.; Borah, P.; Venugopala, K. N.; Bataineh, Y. A.; Al Khames Aga, Q. A. Anticancer Activity and in Silico ADMET Properties of 2,4,5-Trisubstituted thiazole Derivatives. *Curr. Drug Metab.* **2020**, *21*. https://doi.org/10.2174/1389200221666201217094602.